ELSEVIER

Materials Science and Engineering A 422 (2006) 115–122

MATERIALS SCIENCE & ENGINEERING A

www.elsevier.com/locate/msea

Molecular dynamics simulations of the atomistic structure of the intergranular film between silicon nitride grains: Effect of composition, thickness, and surface vacancies

Stephen H. Garofalini *

Interfacial Molecular Science Laboratory, Department of Materials Science and Engineering, Rutgers University, Piscataway, NJ 08559, United States

Received 22 February 2005; received in revised form 16 November 2005

Abstract

Molecular dynamics computer simulations were used to study the atomistic structure of intergranular films (IGFs) between two basal oriented Si_3N_4 crystals or between combined basal and prism oriented crystals. Ordering of the ions into the IGF induced by the crystal surfaces was observed using density profiles of the ions, although that ordering is effected by the roughness of the crystal surface. Density profiles of the sum of all ions misleadingly shows a rapid decay in the density oscillations and apparent ordering into the IGF. However, this is an artifact of the coincidence of the maximum in the peaks of one species with the minimum of another species and the actual oscillations of individual species extend into the IGF farther than the sum profile indicates. This result would have important implications regarding the density oscillations observed in physical experiments with regard to the actual extent of ordering into the IGF induced by the crystal surface.

Keywords: Molecular dynamics simulations; Interfaces; Structure

1. Introduction

Polycrystalline ceramics often contain a glassy intergranular film (IGF) between the crystals that occupies only a small volume percentage of the bulk ceramic, but can influence various mechanical, thermal, chemical, and optical properties. As such, there have been a large number of studies to determine the structure and behavior of these IGFs [1–17]. However, the glassy nature of the IGF and its very thin width between crystals make understanding the atomistic structure and fundamental behavior of IGFs experimentally formidable, although recently there have major experimental breakthroughs [7,15,17]. These recent high resolution electron microscopy (HREM) studies are beginning to provide specific information with respect to the detailed atomistic structure near the IGF/prism interface in silicon nitride [7,15]. Another recent study provides for the pair distribution function (PDF) of the Si–O interactions in the amorphous IGF between silicon nitride crystals [17].

The application of computational techniques offers an important complementary approach to such experimental studies for understanding the structural and kinetic properties of these systems. Computational studies have been used to address the atomistic structure of IGFs between oxide and nitride crystals [14,18–31]. The ab initio calculations provide very specific information over small numbers of atoms, thus giving details about preferential bond formation; the classical simulations provide details of atomistic behavior over larger system sizes and longer times. For instance, the ab initio method has been used to show the energetic differences between specific types of bond clusters of Al, Si, O, and N in silicate IGFs between nitride crystals [14,16], thus enabling interpretation of interfacial bonding and its effect on debonding. The MD simulations enable some direct comparisons to experimentally obtained data, such as structural data, activation energies for diffusion, and spatial distributions of specific species within the IGF.

Our earliest simulations of silica, calcium silicate, and sodium silicate IGFs between ideal α-Al_2O_3 (0 0 0 1) planes showed an ordered cage-like structure forming at the IGF/crystal interface that is enhanced by the presence of the alkali and alkaline earth cations [18,19,21]. Fig. 1 shows an example of the

* Tel.: +1 732 445 2216; fax: +1 732 445 3258.
E-mail address: shg@glass.rutgers.edu.

0921-5093/$ – see front matter © 2006 Elsevier B.V. All rights reserved.
doi:10.1016/j.msea.2006.01.009

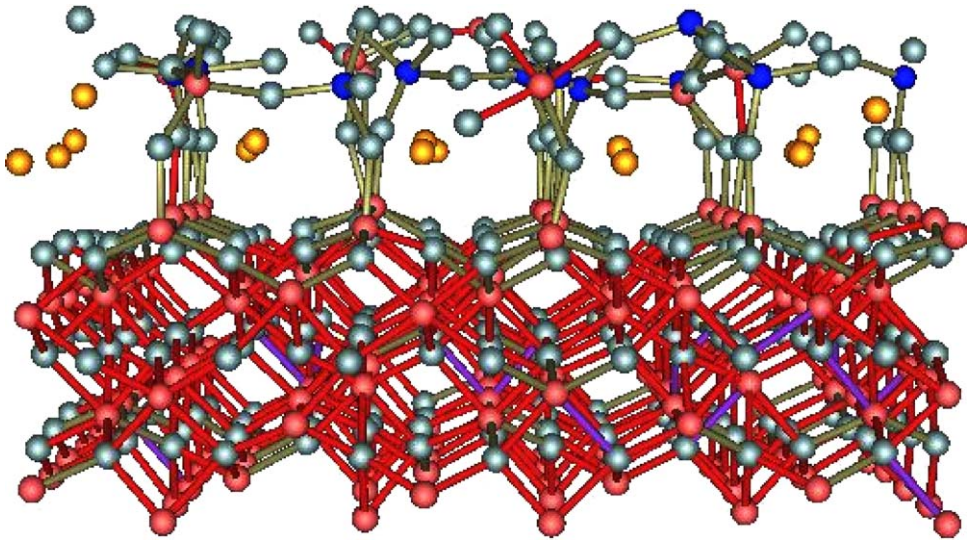

Fig. 1. Snapshot of the side view of a portion of the IGF/(0 0 0 1) alumina interface, showing the ordered cage-like structure at the interface facilitated by the preferential segregation of Ca within the cages. Al, red; O, grey; Si, blue; Ca, yellow.

structure occurring at the interface between the IGF/(0 0 0 1) Al terminated alumina crystal surface. This order is caused by the presence of the coordinatively undersaturated ions on the crystal surface that readily interact with the ions in the glassy IGF. O ions from the IGF readily attach to the terminal Al from the crystal. These O are also attached to Si towards the IGF, forming the cage. The Ca ions preferentially enter the cage in order to satisfy the undercoordinated O in the crystal surface and the zeolitic-like O in the cage sides. These 'zeolitic O' are similar to those O ions found in alumino-silicate zeolites, where the O attached to an Al in the tetrahedral site requires an additional charge compensating cation nearby. In the IGF system shown here, the Ca ions perform this function. Si could have entered into the cage in lieu of the Ca, but the tetrahedral bonds from that Si to the O would be unduly strained and the Si are not stable in such sites. Clarke had previously proposed an ordered interface structure in order to explain the uniformity of IGF thickness [32]. Our initial simulations clearly showed the atomistic details of the IGF/alumina structure and the important role of the modifier cations (Ca in particular) on the structure and mechanical properties of the system [18,19].

These simulation results also showed the implications of such adsorption on the inhibition of growth of the basal plane in the direction of the surface normal, $\vec{n}(0\,0\,0\,1)$. Additional simulations were performed using two different alumina crystals with different surface orientations in contact with the same calcium alumino-silicate IGFs [27,33]. As shown in Fig. 2, results consistently showed little adsorption of Al onto the (0 0 0 1) surface with different IGF compositions, with the highest alumina concentration in the IGF at the anorthite composition. As also shown in Fig. 2, these simulations showed adsorption of Al (and O, not shown) onto the $(1\,1\,\bar{2}\,0)$ plane, increasing with increasing Al concentration in the IGF [27,33]. Such simulation results indicate preferential growth of the $(1\,1\,\bar{2}\,0)$ plane in the $\langle 1\,1\,\bar{2}\,0\rangle$ direction, but little growth of the basal plane in the $\langle 0\,0\,0\,1\rangle$ direction, which is consistent with experimental studies of anisotropic grain growth in alumina.

In the work presented here, a summary of some of the results of the structures observed in the IGFs between silicon nitride crystals will be presented as well as new data regarding roughened IGF/crystal interfaces.

2. Computational procedure

In all cases, a multibody interatomic potential was used in the MD simulations, which is given as:

$$V = \sum_{i \neq j} V_{ij}^{\mathrm{BMH}} + \sum_{i \neq j \neq k} V_{jik}^{\text{3-body}} \tag{1}$$

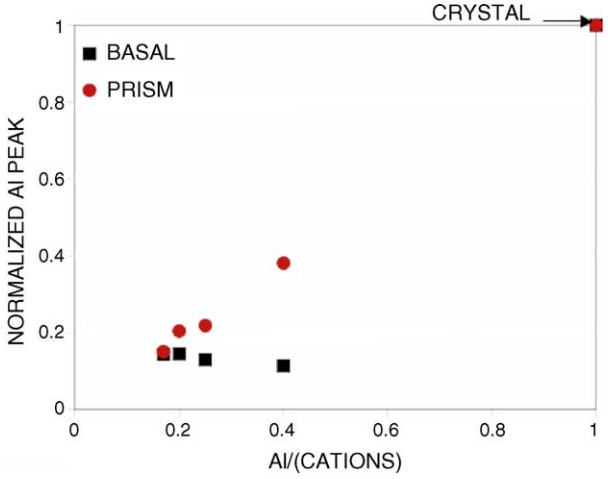

Fig. 2. Ratio of the areas in the density profiles as a function of Al/cation ratio. Area of the first Al peak from the IGF adsorbed onto the basal and prism crystal surfaces normalized by the area of the Al in the crystal plane for the specific crystal orientation.

where V_{ij}^{BMH} is the modified Born–Mayer–Huggins (BMH) pair potential and $V_{jik}^{\text{3-body}}$ is the three-body potential term.

The modified BMH pair potential is given by:

$$V_{ij}^{\mathrm{BMH}} = A_{ij} \exp\left(\frac{-r_{ij}}{\rho_{ij}}\right) + \frac{q_i q_j}{r_{ij}} \xi\left(\frac{r_{ij}}{\beta_{ij}}\right) \quad (2)$$

where r_{ij} is the separation distance between ions i and j, q_i and q_j are taken as full formal charge of the ions, and ξ is the complementary error function which reduces these formal charges as a function of distance between the ion pairs and the value of the screening term β_{ij}.

The three-body term, $V_{jik}^{\text{3-body}}$, is given as:

$$V_{jik}^{\text{3-body}} = \lambda_{jik} \exp\left(\frac{\gamma_{ij}}{r_{ij} - r_{ij}^0} + \frac{\gamma_{ik}}{r_{ik} - r_{ik}^0}\right) \Omega_{jik} \quad (3)$$

when $r_{ij} < r_{ij}^0$ and $r_{ik} < r_{ik}^0$. Otherwise, $V_{jik}^{\text{3-body}} = 0$.

The angular part, Ω_{jik}, is defined as:

$$\Omega_{jik} = (\cos\,\theta_{jik} - \cos\,\theta_{jik}^0)^2 \quad (4)$$

for the (Si/Ca–O–Si/Ca, Si–N–Si, and O/N–Si–O/N), (Si)–(O/N)–(Si), and O–Si–O structure, where θ_{jik} is the angle formed by the ions j, i, and k, with the ion i at the vertex. Since the modifier ion is normally more ionic in these systems, no modifier ion is used as a central ion in the three-body term. The three-body term in this potential biases those species where bond directionality may be involved (currently species like Si, O, Al, B, and N) to a specific angle, but it is fairly weak and does not preclude other coordination. For instance, the species with the strongest three-body term is Si. While Si is biased towards tetrahedral coordination, and in amorphous silica has 99.5% of the Si in tetrahedral coordination in the simulations, we nonetheless do observe the formation of the five-coordinated Si in the trigonal bipyramidal structure during reactions, either with a water molecule or during high temperature diffusion. Five-coordinated Si is seen as a remnant of the melt in rapidly quenched glasses in NMR [34]. The five-coordinated structure we observe is the same as that obtained using molecular orbital (MO) calculations [35]. It is also believed to occur during sol–gel polymerization, which is also what we observe in our simulations of polymerization [36]. Interestingly, we observe a relative time evolution of the Si Q_n species consistent with NMR results [37]. In studies of multicomponent silicate glasses, the three-body term was centered on the network formers, Si, Al, B, (and O), with no such three-body centered on the alkali and alkaline earths in the glasses. The structure of the glasses was consistent with the data obtained from experimental studies of glasses and showed changes in structure consistent with the experimental data [38].

While this multibody potential is relatively simple, it captures many of the important atomistic and macroscopic features of ceramic materials.

For instance, the lowest energy (0 0 0 1) surface in α-alumina is that with a single Al termination layer (as opposed to the O-termination layer or the layer terminating with both layers of Al ions). The single Al termination was also found to be the lowest energy termination plane in ab initio calculations [39,40] and classical MD simulations using different forms of interatomic potentials [41–43]. Our own simulations gave a surface energy for the single Al-terminated (0 0 0 1) surface equal to 2.04 J/m^2 [42], close to the subsequently performed ab initio calculations that put the value at 1.95 J/m^2 [39]; the simulations also gave a significant inward relaxation of the surface Al plane, similar to the ab initio calculations.

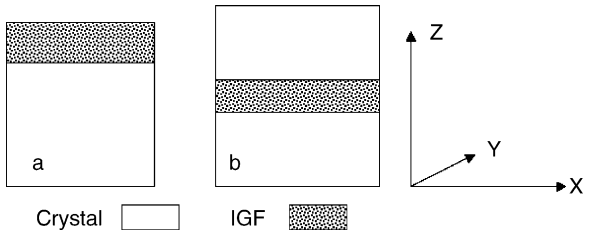

Fig. 3. Schematic drawing of the different set-ups used in the simulations. Periodic boundaries in all three dimensions. Set-up (a) is used for the IGF between the same crystal orientations. Set-up (b) is used when the IGF is between two crystals with different orientations. In (b), an extra vacuum is above the upper crystal to prevent the top on the upper crystal from interacting with the bottom of the lower crystal.

In simulations of silica and silicate glasses, this form of interatomic potential reproduces the bulk and surface structure of silica and silicate glasses and was applied to silicon nitride systems after development of a reasonable potential for the nitride [28].

All systems containing an IGF were made using either of two techniques. If the IGF was situated between the two terminations of a single crystal orientation, then Fig. 3a applied, with periodic boundary conditions in all three dimensions, which allowed the IGF atoms (stippled) to be in contact with both the top crystal surface and the bottom crystal surface. If two dissimilar crystal surfaces were in contact with the same IGF, then Fig. 3b was used, with a vacuum above the top surface to prevent interactions between atoms in the top crystal with atoms in the bottom crystal across a periodic boundary in Z. The crystals in Fig. 3b were ∼5 nm in X, Y, and Z, with ∼14,000 atoms. The IGFs had similar X and Y dimensions, but had thicknesses ∼0.7–2 nm, with the IGF thickness depending on the number of ions in the IGF and composition. Details of the computational procedure have been published [28–30]. These previous simulations of the IGF between nitride crystals used ideally terminated and relaxed crystal surfaces.

More recent simulations have been performed on nitride surfaces where crystal surface vacancy defects have been introduced in order to determine the effect of vacancies and oxynitride formation in the crystal surfaces on the subsequent ordering of ions in the IGF induced by the crystals. The vacancies were introduced into the crystal surfaces by randomly removing a specific number of ions from the first three crystal layers nearest the IGF in the basal oriented silicon nitride crystal. The outermost crystal layer closest to the IGF is labeled layer 1, followed by layers 2 and 3. The percent of ions removed from layers 1, 2, and 3 are 80%, 50%, and 20%, respectively. The ions removed from the crystal were added into the IGF at the onset of formation of

Table 1
Composition of the IGF after adding the atoms removed from the crystal surfaces into the IGF

IGF atom numbers	Crystal surface atoms removal
Si, 1405; O, 2238	Layer 1: 80%
N, 508; Ca, 142	Layer 2: 50%
Total in IGF: 4293	Layer 3: 20%

the IGF so that the stoichiometry of the whole system is retained. The surface crystal vacancies could be filled by ions from the IGF during the melt/quench process of forming the IGF in the simulations. The composition of the IGF is given in Table 1. The glassy IGF is made via a melt/quench procedure using both NVE and NPT ensembles, as shown in Table 2 [28–30]. Two quench procedures were used, one being much longer than the other. However, only slight differences were observed in using the longer Schedule 2 quench in comparison to Schedule 1, as presented below, and the major trends were unaffected.

3. Results and discussion

3.1. Relaxed ideally terminated nitride surfaces

Fig. 4 shows some density profiles perpendicular to the IGF/crystal interfaces in a system containing pure silica in the IGF between two (0 0 0 1) basal oriented silicon nitride crystals. The lighter line depicts the N ions from the crystal and provides an indication as to the end of the crystal on each side of the IGF. The darker solid line is the density profile of the sum of all ions in the system, including those in the IGF. In this orientation, both Si and N are in the same (0 0 0 1) plane in the crystal, giving the larger sum line in the crystal than just the density of the N. Note the large sum peak in the IGF immediately adjacent to the crystal surfaces. This is caused by the epitaxial adsorption of Si and O from the IGF onto the nitride surface, which has been previously discussed [28]. Density oscillations appear to exist into the IGF, but at a much lower intensity than the first adsorbed peak, indicating a relatively rapid dampening of the density oscillations.

Table 2
Melt/quench procedure used for making the glassy IGF between the nitride crystals

Quench temperature, T (K)	Conditions	Time at T (ps)	
		Schedule (1)	Schedule (2)
10000	NVE, crystal frozen	20	20
8000	x, y constant, $P_z = 5$ GPa	200	1000
6000	As above	200	1000
4000	As above	200	1000
3000	x, y constant, $P_z = 3$ GPa, crystal de-frozen	100	500
2000	NPT, $P = 0.1$ MPa	50	50
1000	As above	10	50
300	As above	30	30

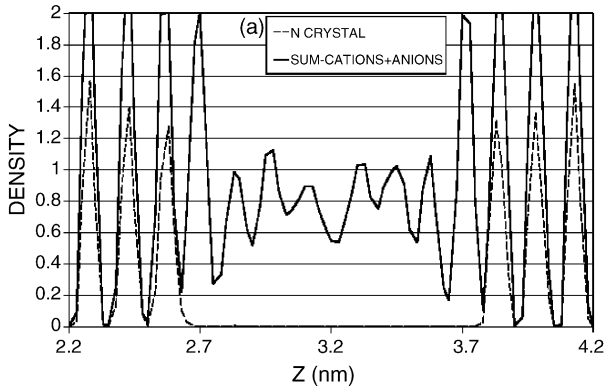

Fig. 4. Density profile as a function of the Z-coordinate of the N ions in the silicon nitride crystals (dashed line to show the location of the crystals) and the sum of all ions in the system for two silicon nitride crystals with the basal planes in contact with the IGF. Only the profiles near the IGF are shown.

However, this may be somewhat misleading, and Fig. 5 provides a more detailed view of the density profiles of the individual species. In Fig. 5, the Si from the IGF (Si-g) and the O show peak intensities in the layer adjacent to the crystal surfaces similar to the Si-c and N values of the first crystal layer. Fig. 5 also shows that the individual Si-g and O species show significant density oscillations into the IGF that would be missed by the summation curve of all ions (Fig. 4). This is because the peaks in the Si-g generally coincide with the minimum in the O curve, and vice versa for the O peaks, smoothing the resultant summation curve. Hence, one of the important advantages of using MD simulations to study these systems is the ability to discriminate between individual species in such density profiles that would currently be unattainable by physical experiments.

Fig. 6 shows a snapshot of a side view of a thin section of a ∼1.6 nm calcium silicate (12% CaO) IGF and a small portion of the two basal oriented silicon nitride crystals adjacent to the interfaces. The relatively strong Si–O (and Si–N) bonds are drawn, showing the connectivity of the two crystals via the siloxane bonds in the IGF. Bonds between Ca to O are not drawn in order to show the relative weakening of the structure caused by the calcia additions (Ca–O bond strength ∼1/3 that of the

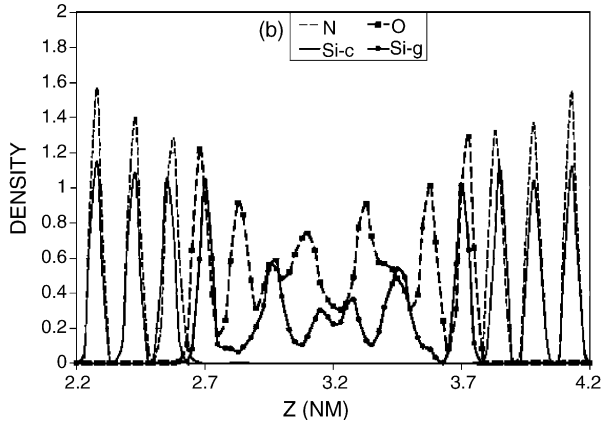

Fig. 5. Individual density profiles of the ions in same system as shown in Fig. 4. Whereas Fig. 4 implied a rapid dampening of the density profile in the IGF, the individual species show density oscillations and ordering throughout the IGF.

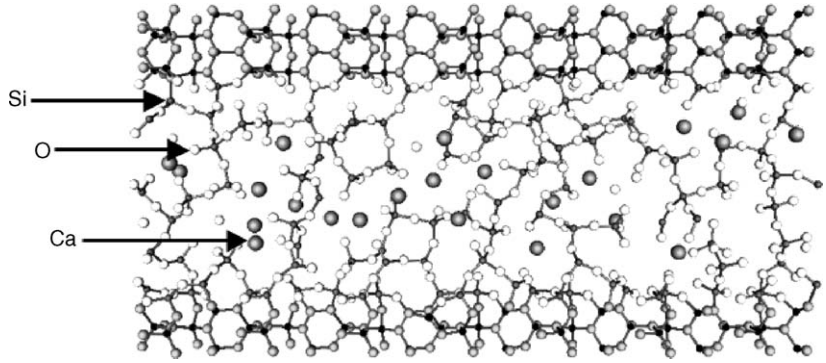

Fig. 6. Snapshot of a thin section into the plane of the image of the region near the interfaces of two basal oriented silicon nitride crystals in contact with a calcium silicate IGF.

Si–O). This weakening of a silicate phase by the incorporation of alkaline earths (and alkali) is well known in glass science and such additives are called network modifiers in that these ions disrupt the strong network bonding of silica. An important feature observed in the simulations relates to the effect of compositional and thickness changes in the IGF on the coordination of the O that are attached to the nitride surface. Fig. 7 shows a side view of a portion of the interface between one basal surface and the calcium silicate IGF. The oxygen are labeled as $O_{i,j}$ in order to distinguish the different type of Si attached to the O, where i denotes the number of Si first neighbors that are attached to the nitride surface, whether they are original Si from the crystal or Si adsorbed from the IGF onto nitride lattice sites, and j represents the number of Si attached to this O that are still in the IGF. The figure also shows that the Si and O from the IGF adsorbed onto the crystal continue the crystal structure. Fig. 8 shows the statistics of the different bonding types of O adsorbed onto the nitride surface. As the figure clearly shows, most O adsorbed onto the nitride surface are two-coordinated, with most being attached to 2Si that are in nitride lattice sites ($O_{2,0}$) or having 1Si in a surface site and 1Si in the glassy IGF ($O_{1,1}$) (also see Fig. 7). The main comparisons in Fig. 8 are between the white and black histograms and between the two hashed histograms.

The white and black histograms differ only in the concentration of CaO in the IGF. With no CaO, there are few one-coordinated O (often called non-bridging O, or NBO) attached to the nitride surface ($O_{1,0}$). However, increasing the CaO concentration causes a dramatic increase in these one-coordinated O, as shown by the $O_{1,0}$ black histogram. These $O_{1,0}$ form at the expense of the $O_{1,1}$, as seen by the sharp decline in such species with increasing CaO content (white to black histograms in $O_{1,1}$). Similarly, thinning the IGF from 1.5 to 0.7 nm, shown in the hashed histograms, shows a sharp increase in $O_{1,0}$, again at the expense of $O_{1,1}$. Because the increased NBO observed in both cases are associated with O attached to the crystal lattice, the implication of these results is that too much CaO in the IGF or too thin an IGF will cause a significant weakening of bonding along the IGF/crystal interface. This localized 'planar' weakening would weaken the connectivity between the two crystal surfaces, which are otherwise attached to each other via the IGF, thus enabling easier separation of the two crystals or easier flow of material. Additional details regarding this behavior and the effect of O coordination at the interface is presented elsewhere [28].

Simulations were also performed using IGFs containing N, which is more realistic than the earlier simulations of pure oxide

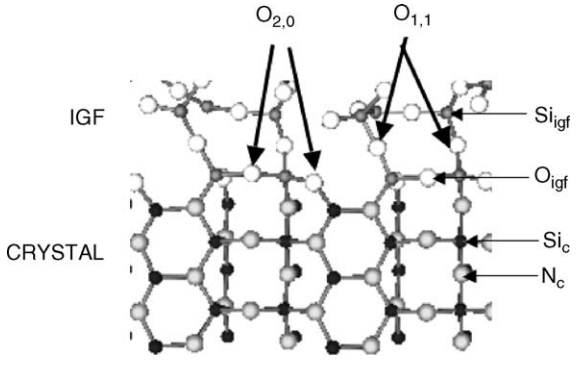

Fig. 7. Snapshot of the a thin section into the plane of the image of a region near the IGF/basal oriented nitride crystal, showing the nomenclature for the different bonding schemes for O attached to at least one Si on the crystal surface. The subscripts on the $O_{i,j}$ indicate (i) the number of Si bonded to this O that are at lattice sites in the crystal and (j) the number of Si bonded to this O that are still in the IGF.

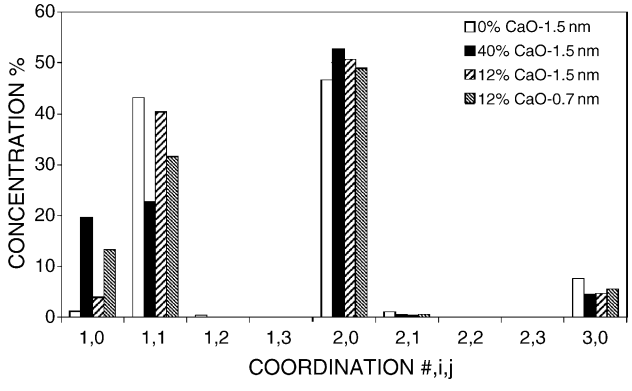

Fig. 8. Concentration of the number of $O_{i,j}$ at the nitride surface as a function of CaO concentration at constant IGF thickness (white and black histograms) or as a function of IGF thickness at constant CaO concentration. Increased CaO concentration or decreased thickness cause significant increases in the concentration of non-bridging oxygen, $O_{1,0}$ at the expense of the $O_{1,1}$, which can affect the connectivity of the contacting grains.

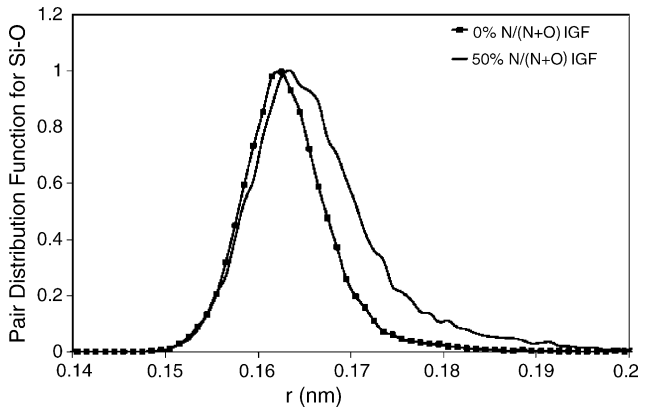

Fig. 9. Normalized pair distribution functions (PDF) for Si–O pairs in the IGF as a function of N in the IGF.

IGFs. The pair distribution function, PDF, for the Si–O peak as a function of the concentration of N in the IGF between a basal (0 0 0 1) oriented crystal and a prism (1 0 $\bar{1}$ 0) oriented crystal is shown in Fig. 9. The peaks are normalized to 1. The addition of N causes an elongation of the Si–O peak as N replace some O in the anion tetrahedron surrounding the Si in the IGF. Experimentally, the Si–O peak in the IGF occurs at 1.64 ± 0.04 Å [17]. The structure of the Si–O bond is affected both by the presence of the interface [30] as well as the presence of N in the IGF, as shown in Fig. 9. Hence, the spread observed in the experimental data would incorporate both effects and again shows the advantage of applying computational techniques to complement physical experiments.

Since there were clearly differences in adsorption (and growth) behavior of Al (and O) from silicate IGFs onto the basal versus prism planes in the alumina system, structure of the IGF that is in contact with both the (0 0 0 1) basal and (1 0 $\bar{1}$ 0) prism planes in the silicon nitride system was evaluated [30]. Results showed behavior opposite to that of the alumina system. Fig. 10 shows the results of simulations of the calcium silicate IGF between a basal oriented crystal on the left in the figure (labeled B), and a prism oriented crystal on the right (labeled P).

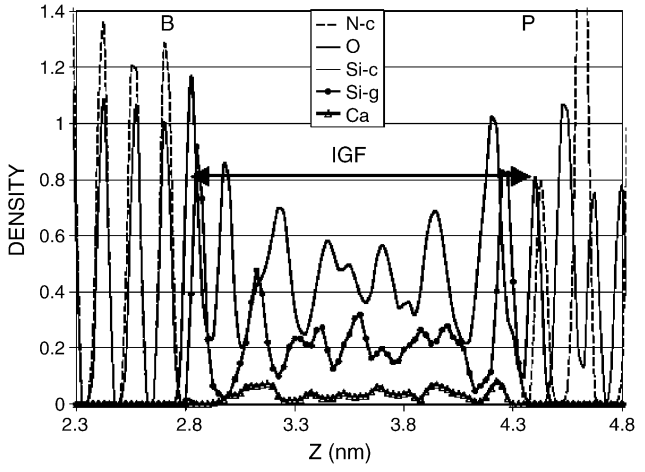

Fig. 10. Density profile near the IGF of individual species of the calcium silicate IGF between the basal oriented crystal (B, on the left) and the prism oriented crystal (P, on the right). Arrow locates the width of the IGF.

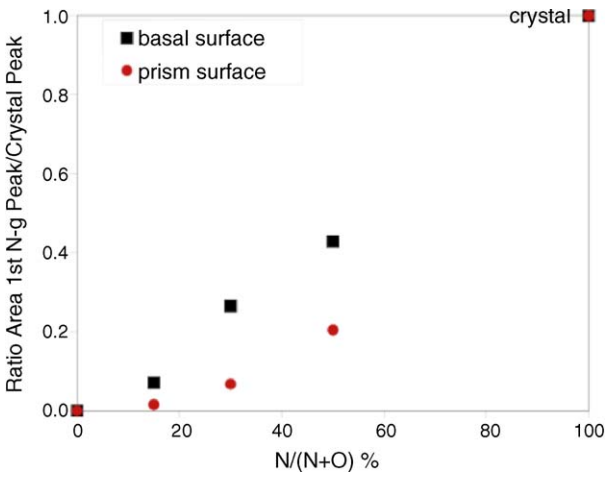

Fig. 11. Ratio of the areas in the density profiles as a function of N to anion ratio in the IGF. Area of the first N peak from the IGF adsorbed onto the basal and prism crystal surfaces normalized by the area of the N in the crystal plane for the specific crystal orientation.

Again, Si-g and O epitaxially adsorb onto the basal side, with no adsorption of the Ca. The termination plane on the (1 0 $\bar{1}$ 0) side is a N layer. O from the IGF adsorb into this layer, completing the anion concentration needed, allowing for cation adsorption. Si-g from the IGF is the next peak into the IGF, but it has competition from the Ca ions that adsorb at the same location (in the *Z*-coordinate). This competition for sites by the two cations is consistent with the most recent HRTEM studies of the structure of the IGF/nitride crystal interface, where Y rather than Ca was studied [7,15]. The main feature of the simulations and the experiments is the competition between Si and the other additives at the prism surface. Such a competition was seen at the basal surface in the alumina system, whereas it is seen on the prism surface and not the basal surface in the nitride system. This adsorption from the IGF affects growth of the crystals.

Fig. 11 shows the area of the first peak of N from the IGF (N-g) adsorbed onto the crystal surfaces divided by the area of the N peak in the crystal. This ratio is used here as a measure of the growth along the surface normal for the basal and prism orientations in the nitride system. As in Fig. 10, the IGF is in contact with both orientations simultaneously. Growth along the basal surface normal is faster than along the prism surface normal. Again, experimental data of abnormal grain growth in silicon nitride occurs with growth along the basal surface normal, $\vec{n}(1\,0\,0\,0)$, being greater than that along the prism surface normal. The simulation results reproduce this experimental trend in silicon nitride, which is opposite to that seen in both the experiments and the simulations of the alumina system.

Therefore, the relatively simple interatomic potentials used in the simulations of the oxide and nitride systems reproduces the experimentally observed trends in growth behavior in each system, even though those trends are opposite.

3.2. Roughened nitride surfaces

The previous studies employed ideally terminated crystal surfaces that were allowed to relax. This created flat crystal surfaces

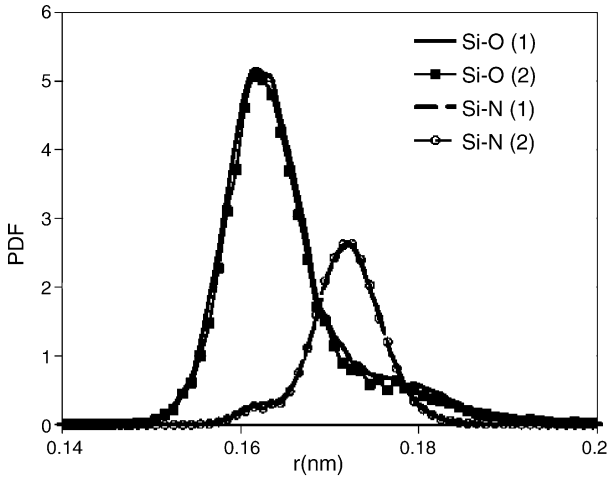

Fig. 12. Pair distribution functions (PDFs) for Si–O and Si–N first peak for the two quench schemes shown in Table 1, showing almost no change in structure with the different quench times.

in contact with the IGF and enabled relatively easy data analysis and interpretation. The simulation results clearly showed the effect of the crystal order on ordering into the IGF, as presented above. Additional simulations were made using defective nitride basal surfaces in order to determine the effect of disorder in the crystal surface and a compositional interphase between the crystal and the IGF on ordering at the interface and into the IGF. As mentioned in Section 2, the nitride basal surfaces on either side of the IGF had ions removed from the first three crystal layers of each and two simulation quenches were studied. The Si, O, and N ions from the IGF had to diffuse into these crystal vacancies, so the different quench rates were used to affect the kinetics. The different quench rates had little or no effect on the structure in the IGF, as shown by the Si–O first peak and Si–N first peak (Fig. 12) and also observed in the longer range PDF structure (not shown). Similarly, the overall features of the density profiles are similar. Fig. 13 shows the results of the longer quench. Ordering

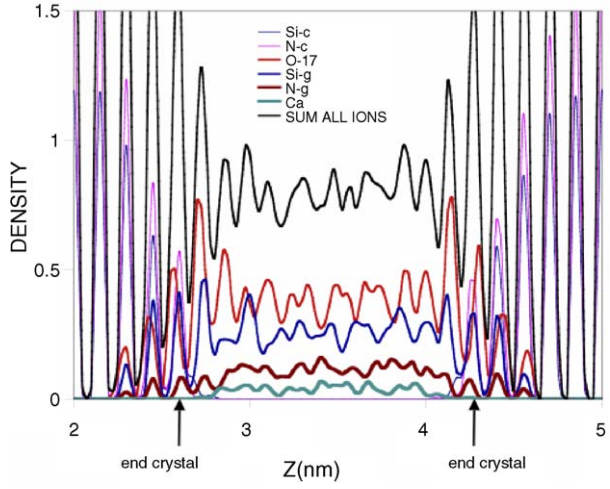

Fig. 13. Density profiles of individual ions and the sum of all ions for simulations of the IGF in contact with two basal oriented silicon nitride crystals that have 80%, 50%, and 20% vacancies introduced into the 1st, 2nd, and 3rd crystal layers from the end of the crystal, respectively.

of the ions into the IGF from the crystal surfaces is not as strong as that observed in the ideally terminated nitride basal crystal surfaces [28–30]. The large concentration of surface vacancies introduced into the outer crystal layer (80%) indicates that such a large disorder and interphase mixing of O into the N lattice sites affects ordering of ions into the IGF. Smaller degrees of disorder might have a lesser effect on ion ordering into the IGF. One implication of such results is that if ordering is experimentally observed in the IGF, then the degree of surface roughness and interphase mixing must be limited to values less than that shown here.

4. Conclusions

Molecular dynamics computer simulations were used to study the atomistic structure of intergranular films (IGFs) between oxide and nitride crystals in order to complement the experimental studies of these systems. Previous simulations of calcium alumino-silicate IGFs between alumina crystals showed ordering at the interface, restricted growth along the (0 0 0 1) plane's surface normal caused by Ca, and growth along the prism plane's surface normal. The results showed that the simulations could reproduce abnormal grain growth in the alumina system in a manner similar to that observed experimentally. This work was extended to the nitride system, where abnormal grain growth occurs differently from the alumina system. Silica, calcium silicate, and calcium silicon-oxynitride IGFs were simulated in contact with nitride crystals. Again, ordering from the interface into the IGF was observed, but evaluation of the summation of the density profile of all ions perpendicular to the interface looks like the order decreases rapidly. However, detailed density profiles of individual species shows that these density oscillations continue more deeply into the IGF and the rapid dampening seen in the total summation is an artifact of the particular periodicity of the individual profiles. The simulations also showed that growth along the $\vec{n}(0\,0\,0\,1)$ direction occurs more rapidly than growth along the $\vec{n}(1\,0\,\bar{1}\,0)$ direction, consistent with that observed experimentally for anisotropic grain growth in silicon nitride. In order to allow for roughening of the nitride crystal surface and oxynitride formation at the interface, vacancies were introduced into the (0 0 0 1) nitride surface layers, followed by long simulations that allowed for mixing between the phases. Results showed that the ordering of the individual species in the IGF was reduced in comparison to the ideally terminated and relaxed nitride surfaces, although the summation profile is similar to the previous work. The results indicate the need for detailed discrimination of the species in experimental studies in order to accurately quantify the induced order into the IGFs.

Acknowledgements

The author is pleased to acknowledge the excellent work of the people associated with this work on IGFs in our lab, Slawomir Blonski, David Litton, Weiwei Luo, Xiaotao Su, and Shenghong Zhang, and acknowledges the most recent support from the NSF Award DMR-0010062 in collaboration with the NANOAM project of EU-CORDIS (G5RD-CT-2001-00586),

as well as partial support from DOE OBES Materials Sciences DE-FG02-00ER45823.

References

[1] I. Tanaka, H.J. Kleebe, M.K. Cinibulk, J. Bruley, D.R. Clarke, M. Rühle, J. Am. Ceram. Soc. 77 (1994) 911–914.
[2] X. Pan, H. Gu, R. van Weeren, S.C. Danforth, R.M. Cannon, M. Rühle, J. Am. Ceram. Soc. 79 (1996) 2313–2320.
[3] H. Gu, X. Pan, R.M. Cannon, M. Rühle, J. Am. Ceram. Soc. 81 (1998) 3125–3135.
[4] H.-J. Kleebe, M.K. Cinibulk, R.M. Cannon, M. Rühle, J. Am. Ceram. Soc. 76 (1993) 1969–1977.
[5] C.-M. Wang, X. Pan, M.J. Hoffmann, R.M. Cannon, M. Ruhle, J. Am. Ceram. Soc. 79 (1996) 788–792.
[6] H. Gu, R.M. Cannon, M. Rühle, J. Mater. Res. 13 (1998) 376–387.
[7] A. Ziegler, C. Kisielowski, M.J. Hoffmann, R.O. Ritchie, J. Am. Ceram. Soc. 86 (2003) 1777–1785.
[8] P.F. Becher, E.Y. Sun, C.-H. Hsueh, K.B. Alexander, S.-L. Hwang, S.B. Waters, C.G. Westmoreland, Acta Mater. 44 (1996) 3881–3893.
[9] P.F. Becher, G.S. Painter, M.L. Lance, S. Ii, Y. Ikuhara, J. Am. Ceram. Soc. 88 (2005) 1222–1226.
[10] P.F. Becher, G.S. Painter, E.Y. Sun, C.H. Hsueh, M.J. Lance, J. Am. Ceram. Soc. 48 (2000) 4493–4499.
[11] S. Ramamurthy, H. Schmalzried, C.B. Carter, Phil. Mag. A 80 (2000) 2651–2674.
[12] C.B. Carter, Y.K. Rasmussen, Acta Met. 42 (1994) 2741.
[13] Y.K. Simpson, C.B. Carter, J. Am. Ceram. Soc. 73 (1990) 2391–2398.
[14] G.S. Painter, P.F. Becher, E.Y. Sun, J. Am. Ceram. Soc. 85 (2002) 65–67.
[15] N. Shibata, S.J. Pennycook, T.R. Gosnell, G.S. Painter, W.A. Shelton, P.F. Becher, Nature 428 (2004) 730–733.
[16] E.Y. Sun, P.F. Becher, C.H. Hsueh, G.S. Painter, S.B. Waters, S.-L. Hwang, M.J. Hoffmann, Acta Mater. 47 (1999) 2777–2785.
[17] W. McBride, D.J.H. Cockayne, J. Non-Cryst. Sol. 318 (2003) 233–238.
[18] S. Blonski, S.H. Garofalini, J. Phys. Chem. 100 (1996) 2201–2205.
[19] S. Blonski, S.H. Garofalini, J. Am. Ceram. Soc. 80 (1997) 1997–2004.
[20] D.A. Litton, S.H. Garofalini, J. Mater. Res. 14 (1999) 1418–1429.
[21] D.A. Litton, S.H. Garofalini, J. Am. Ceram. Soc. 83 (2000) 2273–2281.
[22] C.M. Marian, M. Gastreich, J.D. Gale, Phys. Rev. B 62 (2000) 3117–3124.
[23] M. Yoshiya, K. Tatsumi, I. Tanaka, H. Adachi, J. Am. Ceram. Soc. 85 (2002) 109–112.
[24] G. Pezzotti, G.S. Painter, J. Am. Ceram. Soc. 85 (2002) 91–96.
[25] G.S. Painter, P.F. Becher, H.-J. Kleebe, G. Pezzotti, Phys. Rev. B 65 (2002), 064113-1-11.
[26] W.-Y. Ching, S.-D. Mo, Y. Chen, J. Am. Ceram. Soc. 85 (2002) 11–15.
[27] S.H. Garofalini, S. Zhang (Eds.), Mater. Res. Soc. Symp. Proc., vol. 751, Materials Research Society, Pittsburgh, PA, Boston, 2003, pp. 191–200.
[28] S.H. Garofalini, W. Luo, J. Am. Ceram. Soc. 86 (2003) 1741–1752.
[29] X. Su, S.H. Garofalini, J. Mater. Res. 19 (2004) 3671–3678.
[30] X. Su, S.H. Garofalini, J. Mater. Res. 19 (2004) 752–758.
[31] P. Rulis, J. Chen, L. Ouyang, W.-Y. Ching, X. Su, S.H. Garofalini, Phys. Rev. B 71 (2005), 235317-1-10.
[32] D. Clarke, J. Am. Ceram. Soc. 70 (1987) 15–22.
[33] S. Zhang, S.H. Garofalini, J. Am. Ceram. Soc. 88 (2005) 202–209.
[34] J.F. Stebbins, P. McMillan, J. Non-Cryst. Sol. 160 (1993) 116–125.
[35] J.D. Kubicki, Y. Xiao, A.C. Lasaga, Geochim. Cosmochim. Acta 57 (1993) 3847–3853.
[36] G. Martin, S.H. Garofalini, J. Non-Cryst. Sol. 171 (1994) 68–79.
[37] S.H. Garofalini, G. Martin, J. Phys. Chem. 98 (1994) 1311–1316.
[38] S.H. Garofalini, in: R. Cygan, J. Kubicki (Eds.), Reviews in Mineralogy and Geochemistry: Molecular Modeling Theory: Applications to the Geosciences, vol. 42, Mineralogical Society of America, Washington, DC, 2001, pp. 131–164.
[39] I.G. Batirev, A. Alavi, M.W. Finnis, T. Deutsch, Phys. Rev. Lett. 82 (1999) 1510–1513.
[40] I.G. Batirev, A. Alavi, M.W. Finnis, Faraday Discuss. 114 (2000) 33–43.
[41] W.C. Mackrodt, R.J. Davey, S.N. Black, R. Docherty, J. Cryst. Growth 80 (1987) 441–446.
[42] S. Blonski, S.H. Garofalini, Surf. Sci. 295 (1993) 263–274.
[43] N.H. de Leeuw, S.C. Parker, J. Am. Ceram. Soc. 82 (1999) 3206–3216.